Article

# Rapid Growth of the $CO_2$ Hydrate Induced by Mixing Trace Tetrafluoroethane

Tianyi Song, Jinhai Zhang,* Wei Li, Jie Ma, Shen Hu, Jianxiu Liu, Xiaonan Li, Wenfeng Hu,
Chunming Lan, Guohua Tian, Tingxiang Jin, Yuexin Han, Jiancheng Wang, Junjie Gong,
and Chuanxiao Cheng*

Read Online

ACCESS | Metrics & More | Article Recommendations

**ABSTRACT:** Rapid formation of the $CO_2$ hydrate can be significantly induced by the gaseous thermodynamic promoter 1,1,1,2-tetrafluoroethane(R134a) due to the mild phase equilibrium conditions, although the formation mechanism and dynamic behavior are not clear. Therefore, a visual experimental system was developed to study the effects of different concentrations of R134a on the induction time, gas consumption, and growth morphology of the $CO_2$ hydrate. At the same time, the combined effects under stirring and sodium dodecyl sulfate (SDS) systems were also studied. In addition, visualization and experimental model diagrams were combined to explain the fast formation mechanism of the R134a/$CO_2$ hydrate. The results show that the $CO_2$ hydrate average conversion rate was increased by more than 63% with the addition of mixed trace R134a(7%). A special phenomenon is found that two temperature peaks appear on the hydrate formation temperature curve, corresponding to two different stages of hydrate formation when stirring or SDS is added to the mixed gas reaction system. Furthermore, the gas consumption in stirring and SDS systems increases by 9 and 44%, respectively. Finally, it is also found that the R134a/$CO_2$ mixed hydrate formed under the action of SDS has a "capillary" mechanism, which provides a gas−liquid phase exchange channel and a large number of nucleation sites for $CO_2$ hydrate, thus promoting the formation of $CO_2$ hydrate. This paper provides a novel, simple, and efficient method for $CO_2$ hydrate gas storage technology.
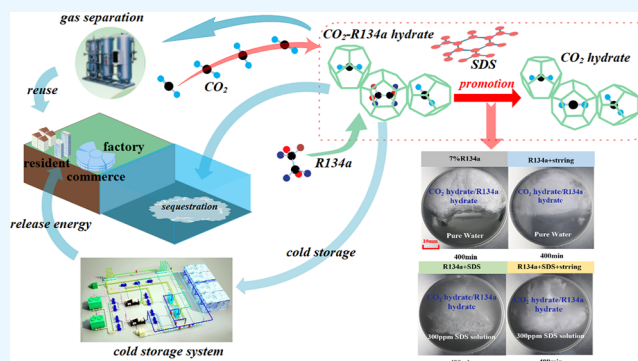
## 1. INTRODUCTION

Carbon dioxide ($CO_2$) emissions from the burning of fossil fuels (coal, oil, and natural gas) are the main contributor to the greenhouse effect. The concentration of global $CO_2$ continues to increase as conventional fossil fuel combustion remains dominant in power and industrial systems.[1] $CO_2$ capture and separation is an important way to reduce carbon emission, whereas mainly industrial separation methods have been distributed into four main techniques: adsorption,[2] absorption,[3] membrane,[4] and cryogenic.[5] Traditional gas separation methods have the problems of high input cost and high energy consumption. It is urgent to develop low-cost methods for $CO_2$ separation and capture.

Hydrates are crystalline compounds formed by hydrogen bonding between water molecules and guest molecules at a specific temperature and pressure. The guest molecules typically include $CH_4$, $CO_2$, and $H_2$.[6] $CO_2$ hydrate is a new method for separation and capture of $CO_2$. It has advantages, such as mild gas separation conditions, no pollution, high purity, and high $CO_2$ storage density.[7] It has been proven that the $CO_2$ hydrate is a potential method for $CO_2$ separation and

capture. $CO_2$ hydrate is an ice-like inclusion substance formed by water molecules and $CO_2$ gas molecules under specific temperature and pressure conditions.[8] Water molecules form cage-like structures through hydrogen-bonding interactions, and the guest molecule, $CO_2$, occupies the cage structure and remains stable under van der Waals force.[9] Due to the selective separation of $CO_2$ hydrate from mixed gas components and the high storage capacity of hydrate for guest molecules, $CO_2$ hydrate has become a new hydrate technology to capture and store $CO_2$ from fuel gas ($CO_2 + H_2$) and flue gas ($CO_2 + N_2$) and to reduce the $CO_2$ emission from power plants to the atmosphere.[10] In addition, due to the high gas storage density and large latent heat of phase transition of $CO_2$ hydrate, its application technology has also attracted extensive attention in
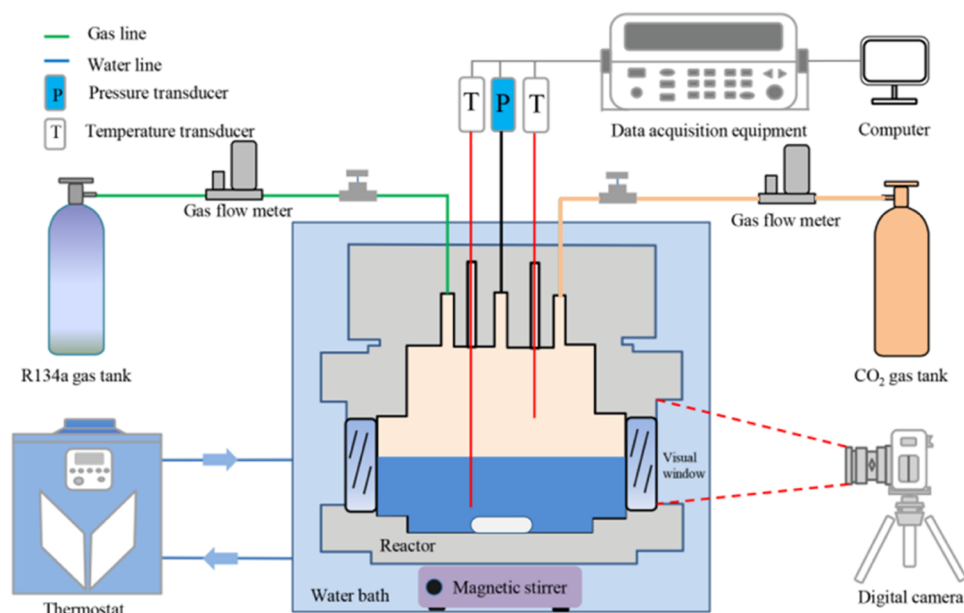
**Figure 1.** System diagram of the experimental device.

the fields of $CO_2$ storage and transportation,[11] cold storage,[12,13] and seawater desalination.[14,15] However, the high operating pressure, slow hydrate formation kinetics, and low hydrate formation rate limit the industrial application of $CO_2$ hydrate technology.[5,16]

In this regard, researchers have focused on the kinetics and thermodynamic properties that promote hydrate formation. In order to reduce the phase equilibrium pressure of $CO_2$ hydrate, tetrahydrofuran (THF) is commonly used as a thermodynamic promoter of $CO_2$ hydrate.[17,18] THF could decline the phase equilibrium condition of ($CO_2$ + THF) mixed hydrates and the induction time of hydrate formation.[19] Lee et al.[20] studied the effect of THF on hydrate formation in a $CO_2$ + $H_2$ mixture. It was found that THF can significantly reduce the phase equilibrium condition and shorten the induction time of hydrate formation. When 1 mol % THF was added to the aqueous solution, the equilibrium hydrate formation pressure changed from about 11 to 1.87 MPa at 278.7 K. Within a specific range (0.5–3 mol %), the hydrate formation rate increased with the increase of THF concentration. One mol % THF has the best promoting effect on hydrate formation. However, above this concentration of THF, the formation of the hydrate will be inhibited. Generally, as a thermodynamic promoter, THF has the problems of low gas consumption and large undercooling. Tetrabutylammonium bromide (TBAB) is another effective thermodynamic promoter to enhance the formation of $CO_2$ hydrate. Li et al.[21] verified the effect of different concentrations of TBAB on the separation and purification of mixed gas ($CH_4$ + $CO_2$) at 2.8 MPa. The experimental results show that 2.57 mol % TBAB has the highest gas absorption and separation efficiency at 6K undercooling. Furthermore, the introduction of SDS into TBAB facilitated the nucleation and growth of hydrate, albeit with diminishing the $CO_2$ separation efficiency. Babu et al.[22] found that when the concentration of TBAB was high, TBAB formed a large semicage hydrate, which hindered the permeability of gas, and the formed dense hydrate layer hindered the diffusion of gas.[23] At present, chemical promoters, such as THF and TBAB, are difficult to recover

and separate. Therefore, finding more efficient methods to facilitate the formation of $CO_2$ hydrates is urgently needed.

The use of gas instead of traditional liquid additives to enhance hydrate formation has been widely studied, providing an update on current research. For example, Yang et al.[14] studied the thermodynamic and kinetic characteristics of $CO_2$−$C_3H_8$ mixed gas hydrate in salt solution with $C_3H_8$ as a hydrate formation promoter. The increasing proportion of $C_3H_8$ significantly reduces the equilibrium pressure of the mixed gas hydrate. This is because the $C_3H_8$ molecule tends to occupy a large cavity to stabilize the hydrate structure, and the formed $C_3H_8$ hydrate can be a promoter for the faster nucleation of other crystals.[24] Wang et al.[25] studied the equilibrium dissociation conditions of $CO_2$ + dichloroethane monofluoride(HCFC-141b)/cyclopentane (CP) hydrate. The experimental results show that the addition of HCFC-141b or CP reduces the equilibrium pressure of the $CO_2$ hydrate. Lee et al.[26] showed that the equilibrium pressure of 2−8 mol % R134a/$CO_2$ mixed ($CO_2$ + R134a) hydrate was 3−5 times lower than that of pure $CO_2$ hydrate. Recent studies have found that the equilibrium pressures of HFCs, such as 1,1-difluoroethane (HFC-152a) and 1,1,1,2-tetrafluoroethane (HFC-134a), are relatively low, and these gases are good hydrate formation promoters (<1 MPa) compared with the conventional hydrocarbon gas hydrates.[27,28] Additionally, the research by Nesterov et al.[29] demonstrated that R134a, as a gas promoter, can significantly reduce the $CO_2$ phase equilibrium pressure. They also discovered that R134a can form SII-type hydrates. In addition, these gas promoters are also easily separated due to the lower liquefaction temperature.[18] Gas promoters have significant effects on declining the pressure of $CO_2$ hydrate formation and increasing the rate of $CO_2$ hydrate formation. However, the mechanism of gas promoter R134a promoting the rapid growth of the $CO_2$ hydrate is unclear.

Therefore, the characteristics of gas promoter R134a facilitating the rapid formation of a $CO_2$ hydrate were systematically investigated in this study. First, under the visualization condition, the growth characteristics of the R134a-enhanced $CO_2$ hydrate are researched, and the optimal

concentration is analyzed by comparing the formation effects of R134a/$CO_2$ at different concentrations. Then, in order to further strengthen the growth rate, the formation morphology and formation rate of the $CO_2$ hydrate reinforced by R134a under stirring and adding SDS are analyzed. Finally, the mechanism of R134a enhancing $CO_2$ hydrate formation in SDS solution is analyzed by a theoretical model and visualization, which provides a theoretical basis for the early realization of industrial application of hydrate technology.

## 2. EXPERIMENTAL MATERIALS AND METHODS

**2.1. Experimental Apparatus and Materials.** The experimental system shown in Figure 1 is mainly composed of a high-pressure reactor, a constant temperature circulating water bath, an image acquisition system, temperature and pressure sensors, and data acquisition system. The stainless-steel pressure reactor volume is 1.2 L. There are two visual windows on both sides, which could withstand a pressure of 10 MPa. A cooling glycol external circulation device (XT5718RC-E800L, Hangzhou Xue zhong Carbon Co., Ltd.) is used to control the temperature in the reactor and provide a low-temperature environment. The measurement range of the temperature sensor (PT-1000, JM608I, Hefei Zhongding Information Technology Co., Ltd.) was −15−200 °C (±0.2%), and the measurement range of the pressure sensor (Unik 5000, PTX5072-TB-A1-CA-H0-PA, General Electric Detection and Control Technology Co., Ltd.) was 0−25 MPa, with an accuracy of 0.25%. The image acquisition system (EOS 6D) was used to record the morphological changes of hydrate formation, and the data acquisition instrument was used to record the data information during the experimental process. The purity of $CO_2$ used was 99.9% (Henan Yuanzheng Technology Development Co., Ltd.); R134a (Shandong Qingdao Sanleng Group Co., Ltd.) and SDS were analytically pure (Shanghai McLean Biochemical Technology Co., Ltd.). All of the solutions used in the experiment were prepared using deionized water (resistivity 16−18 MΩ·cm$^{-1}$).

**2.2. Experimental Method.** The mixture of R134a/$CO_2$ was first prepared by the partial pressure blending method.[5] R134a and $CO_2$ gas were injected into a container in turn. The process was controlled by a gas flow meter and the pressure curve was recorded. These gases were conveyed from the supply vessel to the reactor using a booster pump and subsequently cycled back from the reactor to the supply vessel for several iterations. All gas mixing processes were carried out at a constant temperature to obtain the specified composition, and the partial pressure of $CO_2$ is calculated to be 2.8 MPa.

To represent the formation amount of hydrate during the process of hydrate formation, gas consumption is used. In this process, the inflation of carbon dioxide is slow, and it can be considered that carbon dioxide is saturated in water. Dissolved carbon dioxide can be ignored. This formula was also used in our previous study for calculations.[30] Therefore, the gas consumption is calculated using the following equation[31,32]

$$\Delta n = \left( \frac{PV}{ZRT} \right)_0 - \left( \frac{PV}{ZRT} \right)_t$$

where $P$, $T$, $V$, $Z$, and $R$ (8.314 J·mol$^{-1}$·K$^{-1}$) are the pressure, temperature, and volume of the gas phase in the reactor, the compression factor of $CO_2$ (calculated by the Peng−Robinson equation of state, P−R EOS), and the universal gas constant. $\Delta n$ represents the consumption of $CO_2$. $Z$ is the gas

compressibility calculated by the Pitzer correlation for the second virial coefficient[33]

$$Z = 1 + B^0 \frac{P_r}{T_r} + \omega B^1 \frac{P_r}{T_r}$$

where $P_r$ is the ratio of actual pressure to critical pressure, $T_r$ is the ratio of the actual temperature to the critical temperature, $T_r$ and $P_r$ were obtained by query as 304.2 K and 7.376 MPa, respectively. The equations of Abbott were used for $B^0$ and $B^1$. $B^0$ and $B^1$ are simply functions of the contrasting temperature.[34]

$$B^0 = 0.083 - \frac{0.422}{T_r^{1.6}}$$

$$B^1 = 0.139 - \frac{0.172}{T_r^{4.2}}$$

The calculation of the binary interaction coefficients is provided below since this article involves two different gases. The second virial coefficient responds to the effect of two molecules interacting. The second virial coefficient is calculated by the following equation[34]

$$B = \sum_i \sum_j y_i y_j B_{ij}$$

where $y$ represents the mole fraction of each component in the mixture; $B_{ij}$ represents the interaction between components $i$ and $j$, $B_{ij} = B_{ji}$. For binary mixtures, $B$ is expanded as follows

$$B = y_1^2 B_{11} + 2y_1 y_2 B_{12} + y_2^2 B_{22}$$

where $B$ is calculated by the following equation

$$B_{ij} = \frac{RT_{cij}}{p_{cij}}(B^0 + \omega_{ij}B^1)$$

where $B^0$ and $B^1$ are, as in the above equation, functions of contrast temperature $T_r$; $T_{cij}$, $p_{cij}$, and $\omega$ are calculated according to the following rules

$$T_{cij} = (T_{ci}T_{cj})^{0.5}(1 - k_{ij})$$

$$V_{cij} = \left( \frac{V_{ci}^{1/3} + V_{cj}^{1/3}}{2} \right)^3$$

$$Z_{cij} = \frac{(Z_{ci} + Z_{cj})}{2}$$

$$p_{cij} = \frac{Z_{cij}RT_{cij}}{V_{cij}}$$

$$\omega_{ij} = \frac{(\omega_i + \omega_j)}{2}$$

In the calculation, $k_{ij}$ is taken to be 0. The eccentricity factor is used as a parameter for some measure of the complexity of the shape and polarity of the molecule. The eccentricity $\omega$ factor is estimated by the Edmister method

$$\omega = \frac{3}{7} \frac{\frac{T_b}{T_c}}{1 - \frac{T_b}{T_c}} \log p_c - 1$$
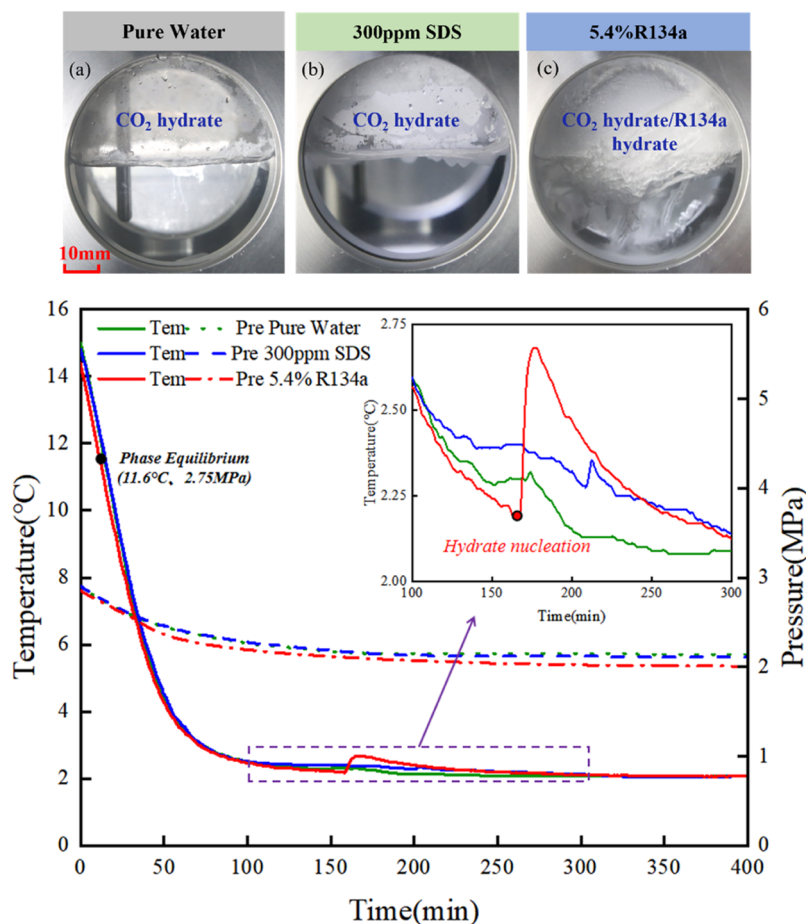
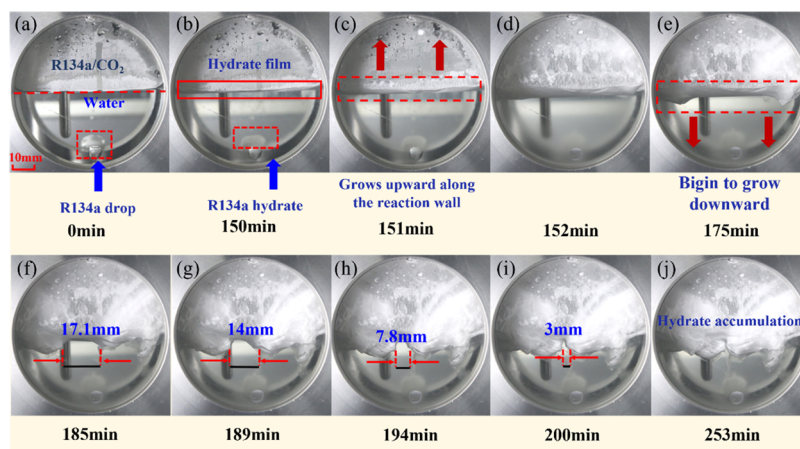**Figure 2.** $P-T$ curve and growth pattern of $CO_2$ hydrate formation with or without R134a.



**Figure 3.** 5.4%R134a/94.6%$CO_2$ hydrate growth process in pure water.

where $T_b$ is the normal boiling point, $T_c$ is the critical temperature, and $p_c$ is the critical pressure. $T_b$ is 275 K, $T_c$ is 304.2 K, and $p_c$ is 3.54 MPa in this paper.

The formation of hydrates in the pure water system, SDS additive system, and trace R134a system was carried out. The data acquisition instrument was used to record the hydrate formation time, temperature, and pressure changes. Then, the gas consumption during the hydrate growth process is calculated by the collected data. The initial temperature $T_0$ of the experiment was 288 K, the set temperature of the experiment was 274.15 K, the average cooling rate was 0.2 K/

min, and the partial pressure of $CO_2$ in the experiment was 2.8 MPa, which ensured the consistency of $CO_2$ content in the experiment. According to the start-up cooling time of the visual reactor, the induction time was judged by the exothermic peak of the pressure drop curve and temperature cooling curve in the reactor.[13]

Before the experiment started, the reactor was cleaned with deionized water, and then, 400 g of deionized water or 400 g of SDS solution (300 ppm) was added to the reactor, which was then placed in ethylene glycol solution. The reactor was washed 3 times with the prepared R134a/$CO_2$ mixture to drain

the air from the reactor. The water bath was initially set to a temperature of 15 °C. Subsequently, the mixture gas was slowly injected to reach the preset pressure, followed by adjusting the water bath temperature to the experimental temperature. After maintaining constant pressure and temperature for approximately 10 h (with a pressure drop of less than 0.01 MPa/h), indicating no further gas consumption, it was considered that the hydrate formation was complete, and the experiment concluded.[28] During the experiment, the change in hydrate formation in the reaction process was recorded by a camera, and temperature and pressure data in the reactor were automatically recorded by a data recorder every 30 s.

## 3. EXPERIMENTAL RESULTS

### 3.1. Trace R134a Promoted the Rapid Formation of $CO_2$ Hydrate.
The formation characteristics of $CO_2$ hydrate in a pure water system, an SDS additive system, and a traced R134a system were studied and compared. The $P-T$ curve and growth process of hydrate in SDS solution, water, and the R134a/$CO_2$ system are shown in Figure 2. It can be seen that the formation rate of pure $CO_2$ hydrate in pure water and SDS solution is very slow. Only a thin hydrate film was observed on the liquid surface when hydrate formation was completed, and the whole growth process took up to 350 min. In the 5.4% R134a system, the final form of hydrate formation in 350 min is shown in Figure 2c. After the addition of R134a, the amount of hydrate formation significantly increased and the formed hydrate fills the whole upper space, with a large amount of hydrate existing in the solution.

In the 5.4% R134a/94.6% $CO_2$ system, the visualization formation morphology of the hydrate is shown in Figure 3. There were three stages for the formation of the R134a/$CO_2$ hydrate. In the initial stage (Figure 3b), thin hydrate films were preferentially formed on the surface of the liquefied R134a droplet at the bottom and at the gas–liquid interface due to the milder phase equilibrium conditions of R134a. In the second stage (Figure 3c), the hydrate gradually formed at the gas–liquid–solid interface and grew in the upper space. The hydrate grew to the entire upper visible window after 152 min (Figure 3d). In the third stage (Figure 3e), the hydrate layer began to form from the gas–liquid boundary toward the solution, corresponding to the temperature rise in the $P-T$ curve in Figure 2. Then, hydrates began to form from the reactor wall toward the center (Figure 3f). When the experiment had lasted for 253 min, the hydrate on both sides grew together, and the hydrate formation was completed.

Trace R134a promoted the rapid formation of the $CO_2$ hydrate. It was found that a higher temperature increase appeared in the $P-T$ curve of the $CO_2$ hydrate formation by mixing trace R134a. It was observed through visualization that the amount of hydrate formation increased significantly, and the hydrate formation became more dense. The average gas consumption of 5.4%R134a/94.6%$CO_2$ hydrate was 0.280 mmol/mol water. The gas consumption is 6.25% higher than that without R134a. This higher gas consumption can be attributed to the preferential formation of hydrates due to the presence of R134a gas, which exhibits a lower phase equilibrium pressure. This, in turn, induces the formation of the $CO_2$ hydrates. In the mixed gas system, R134a gas predominantly forms structure II hydrate. In this scenario, $CO_2$ gas molecules occupy hydrate cages within the R134a hydrate structure. The presence of R134a acts as a thermodynamic promoter, causing the hydrate phase equilibrium line to shift

toward higher temperatures. This, in turn, increases the temperature difference driving force for hydrate formation. Moreover, the increased driving force of hydrate nucleation within the R134a/$CO_2$ hydrate system promotes the formation of R134a/$CO_2$ hydrate, as supported by previous studies.[35]

### 3.2. Hydrate Formation Characteristics of R134a/$CO_2$ Mixtures with Different Concentrations.
In order to study the effect of R134a gas on promoting the formation of $CO_2$ hydrate, experiments were conducted using R134a/$CO_2$ hydrate with different concentrations (5.4−8%) to analyze the enhancement effect and occurrence form of R134a/$CO_2$ hydrate. The $P-T$ diagram of the hydrate formation process is shown in Figure 4. Comparing the hydrate formation at
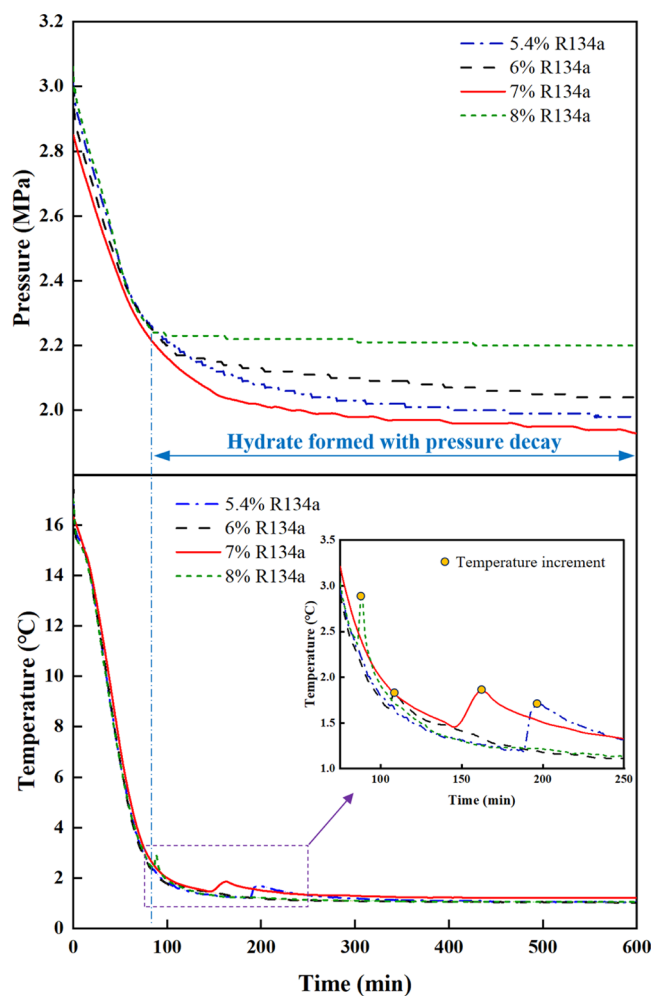


**Figure 4.** $P-T$ curves of hydrate formation with different concentrations of R134a/$CO_2$.

different concentrations of the R134a/$CO_2$ mixture, it was observed that with an increase in the R134a concentration ratio, the final pressure of the reactor is lower, indicating that more $CO_2$ gas is converted into hydrate.

The growth characteristics of different concentrations of R134a/$CO_2$ hydrate in pure water are shown in Table 1. Different concentrations of R134a can enhance the formation of $CO_2$ hydrate, and the induction time is stable within 200 min. The gas consumption of 7%R134a/93%$CO_2$ hydrate formation is the largest. When the concentration of the R134a/$CO_2$ mixture is 1−7%, the induction time of hydrate formation gradually decreases and the gas consumption increases with the

**Table 1. Induction Time and Gas Consumption of Different Concentrations of R134a/CO₂ Hydrate Formation**

| reaction system | $P_0$ (MPa)/ $T_0$ (K) | induction time (min) | average gas consumption (mmol/mol water) |
|---|---|---|---|
| 5.4%R134a/93.6%CO₂ | 3.0/288 | 110/105/115 | 0.280 |
| 6%R134a/94%CO₂ | 3.0/288 | 162/150/170 | 0.282 |
| 7%R134a/93%CO₂ | 3.0/288 | 113/120/123 | 0.302 |
| 8.5%R134a/91.5%CO₂ | 3.0/288 | 141/152/145 | 0.243 |

increase of the concentration. This is because R134a, acting as a thermodynamic accelerator, shifts the R134a/CO₂ hydrate phase equilibrium line toward higher temperatures as the concentration of R134a in the gas phase increases. Consequently, the temperature difference driving force for hydrate formation intensifies, thereby enhancing the driving force for hydrate nucleation in the R134a/CO₂ hydrate system. At the same time, a decrease in the equilibrium pressure of the hydrate formation phase provides a greater pressure driving force. Therefore, more CO₂ hydrate is formed, and the gas consumption per mole of water increases. When the concentration of R134a/CO₂ is greater than 7%, the promotion effect gradually decreases, that is, the induction time increases and the gas consumption decreases. This is because when the concentration of R134a is low, the formed R134a hydrate provides a large number of nucleation sites for the growth of the CO₂ hydrate and increases heat and mass transfer, thus enhancing the CO₂ growth. When the concentration of R134a is too high, a dense R134a hydrate layer is formed at the gas—liquid interface. Although it can provide nucleation sites, it also obstructs the gas—liquid exchange of the CO₂ hydrate, and the upper gas phase cannot supply the CO₂ gas continuously. Therefore, the formation of the CO₂ hydrate is incomplete, and the strengthening effect is reduced.

**3.3. Rapid Formation Characteristics of R134a/CO₂ Hydrate with Stirring or SDS.** In order to increase the gas consumption of CO₂ hydrate, the promoting effects of stirring and SDS were further investigated and compared. When stirring and adding 300 ppm of SDS, the gas consumption during CO₂ hydrate formation increases by 9 and 44%, respectively. Notably, a special phenomenon was found: when stirred or when 300 ppm of SDS was added, there were two temperature peaks on the hydrate formation temperature curve, and the increase in temperature indicates hydrate formation. When SDS was added or stirring was applied, the difference in temperature increase between the two methods was 40 and 120 min, respectively. The first temperature increase peak was due to the formation of R134a/CO₂ mixed hydrate, and the second temperature increase peak corresponded to the formation of CO₂ hydrate (pressure reduction in the P−T curve). The data analysis of the gas chromatograph is shown in Figure 5, and it shows that the R134a gas content decreases significantly at the beginning of hydrate formation, which further confirms the previous conjecture. R134a hydrate is formed in the mixed gas and regenerates into a CO₂ hydrate.

In order to get the nucleation and formation mechanism of 7%R134a/93%CO₂ hydrate, a gas chromatograph was used to analyze the content change of R134a in the gas phase during the reaction process. The concentration of R134a in the mixed gas before and after the experiment was determined by gas chromatography, as shown in Figure 5. During the experiment, the concentration of R134a increased from 0 to 140 min
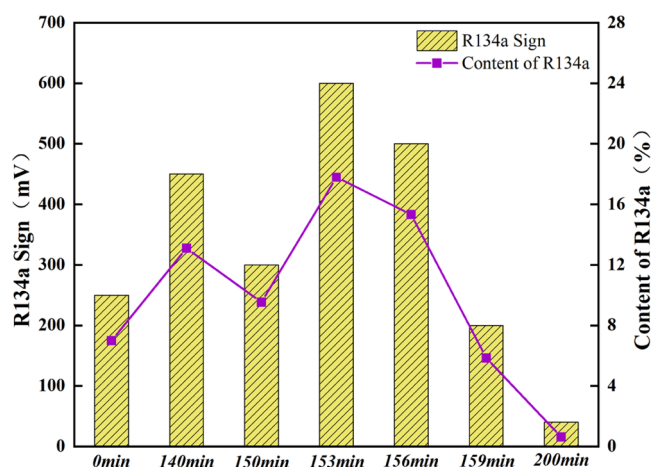


**Figure 5.** R134a gas concentration was detected by a gas chromatograph.

(water bath reduced to 3 °C) because CO₂ is dissolved during the cooling process. At the beginning of the mass formation of the reaction, R134a hydrate preferentially formed a hydrate film at the gas—liquid interface, resulting in a decrease in the concentration of R134a from 140 to 150 min (when the hydrate started mass formation). Subsequently, both CO₂ hydrate and R134a hydrate formed simultaneously, leading to a gradual decrease in the content of R134a at 153 min (3 min after hydrate formation), 156 min (6 min after hydrate formation), and 159 min (9 min after hydrate formation). At 200 min (the end of the reaction), the content of R134a decreased to 0.63%. The change in the concentration of R134a during the formation process was detected by gas chromatography. R134a hydrate was formed and consumed part of the R134a gas, and the R134a hydrate formed acted as a promoter for the massive formation of the CO₂ hydrate, leading to the continuous formation of both hydrates. By the end of the experiment, R134a was almost completely consumed.

Gas chromatography results showed that in the R134a/CO₂ system, R134a in the reactor preferentially formed a hydrate, which further promoted the rapid conversion of CO₂ in the reactor into a CO₂ hydrate. Due to the mild phase equilibrium condition of R134a, the temperature difference driving force of the nucleation of mixed hydrate is higher, and it is easier to form the R134a/CO₂ mixed hydrate.

In order to further increase the gas consumption of CO₂ hydrate, the promotion effect of agitation and SDS on the formation of R134a/CO₂ hydrate was studied. The formation forms of hydrate are shown in Figure 6 (a: 7%R134a; b: 7% R134a + stirring; c: 7%R134a + 300 ppm of SDS; d: 7%R134a + 300 ppm of SDS + stirring). Compared with the hydrate growth morphology without stirring and SDS (Figure 6a), the formed hydrate after stirring is denser, and the hydrate could form in the solution simultaneously. Stirring enhances gas—liquid exchange, reinforces heat and mass transfer at the gas—liquid surface, accelerates the dissolution of CO₂, improves the formation kinetics of the hydrate, and ensures more complete hydrate formation. Figure 6c shows the formation of hydrates in 300 ppm of SDS solution. Compared with pure water and stirring, the thickness of the CO₂ hydrate formation increases. Meanwhile, flocculent hydrate forms in the solution, and the gas consumption of the CO₂ hydrate formation increases. The gas consumption during the CO₂ hydrate formation is shown in Figure 7. In this experiment, compared with pure CO₂
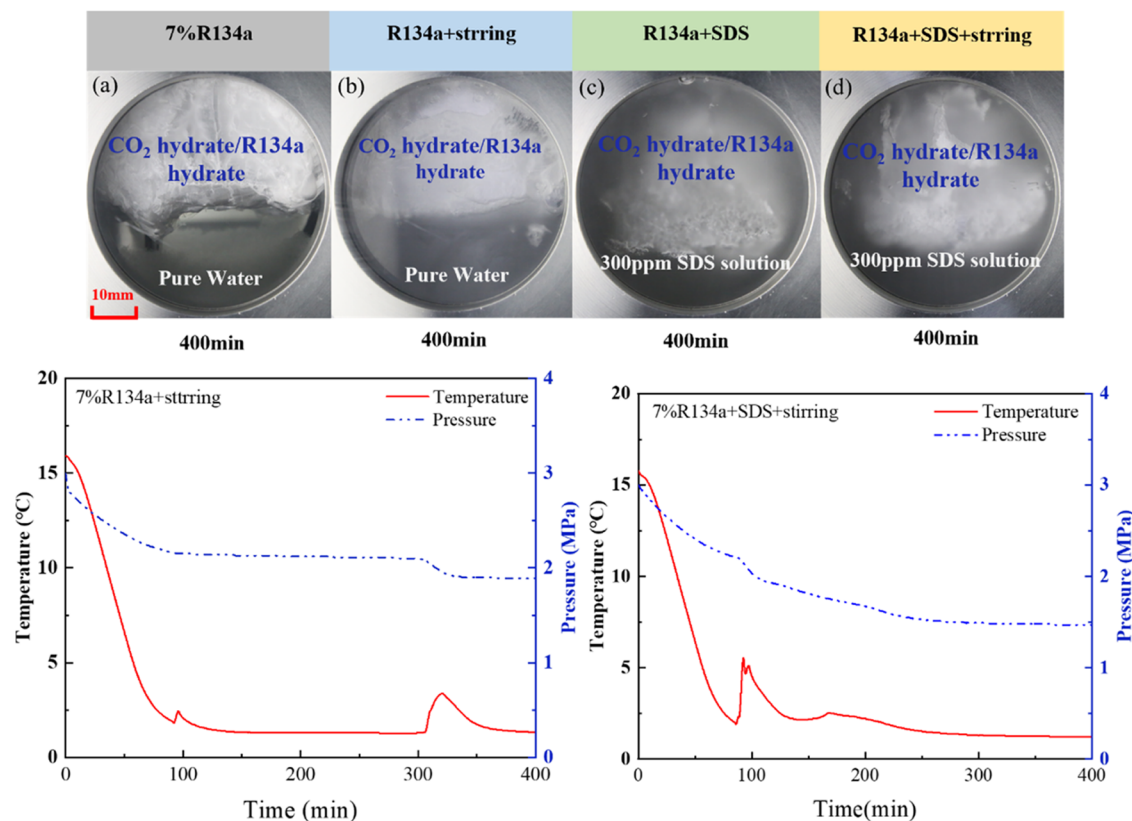
**Figure 6.** $P-T$ of 7%R134$a$/93%$CO_2$ hydrate formation (a: 7%R134a; b: 7%R134a + stirring; c: 7%R134a + 300 ppm of SDS; d: 7%R134a + 300 ppm of SDS + stirring).
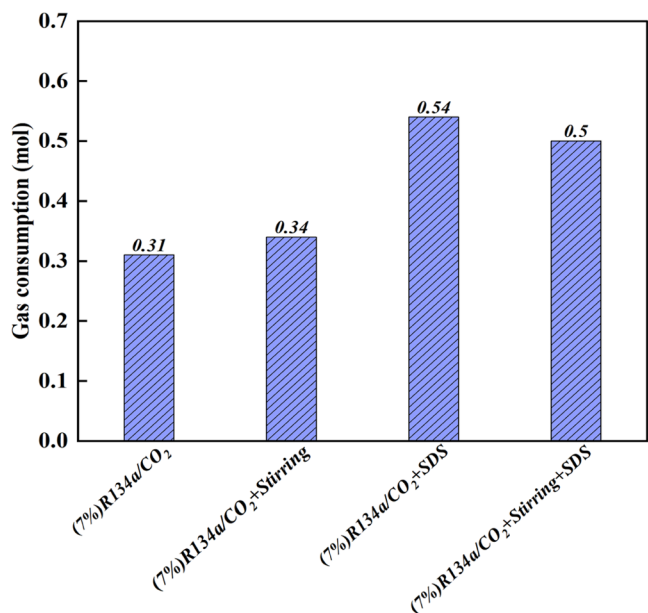


**Figure 7.** Gas consumption of 7%R134$a$/93%$CO_2$ hydrate formation.

hydrate in pure water, the addition of trace R134a induces the formation of a R134a/$CO_2$ mixed gas hydrate, which promoted the nucleation of the $CO_2$ hydrate. The calculation results showed that when stirring and adding 300 ppm of SDS, the gas consumption during $CO_2$ hydrate formation increases by 9 and 44%, respectively.

Based on the remarkable effect of R134a on enhancing the $CO_2$ hydrate in SDS solution, the formation mechanism of R134a-enhanced $CO_2$ hydrate in SDS solution was analyzed by visualization. The visual observation process of the formation of 7%R134$a$/93%$CO_2$ hydrate in 300 ppm of SDS solution is shown in Figure 8. At the initial stage of hydrate formation (Figure 8b), a thin R134a hydrate film appeared at the gas–liquid interface of the reactor due to the milder phase equilibrium of R134a. Under saturation pressure, a small amount of flocculated R134a hydrate appeared below the liquid level. Subsequently, under the promotion of R134a, the $CO_2$ hydrate grows in the upper space from the gas–liquid interface (Figure 8d). The solution becomes cloudy due to the formation of $CO_2$ hydrate in the solution (Figure 8e). With the continuous formation of the $CO_2$ hydrate, the water in the solution is gradually consumed, resulting in the continuous reduction of the liquid level. Hydrate growth reached the whole visual window at 158 min (Figure 8h). In addition, the $P-T$ curve shows that the hydrate growth ended at 163 min. Under the action of SDS, the density of the R134a/$CO_2$ hydrate is higher, and the growth is more uniform throughout the reactor, which solves the shortcoming of R134a/$CO_2$ mixed gas hydrate growing only near the gas–liquid interface. Under the action of 300 ppm of SDS, more $CO_2$ was converted to hydrate, and the average gas consumption of 7%R134$a$/93%$CO_2$ hydrate was 0.54 mmol/mol water.

The gas composition after completion of the formation was analyzed by visual experiments and gas chromatography. The formation model of R134a/$CO_2$ hydrate under SDS conditions was summarized.[31] R134a begins to form hydrate from the gas phase, while the $CO_2$ hydrate is formed from dissolved gas at the gas–liquid interface (hydrate precipitation may also occur in the liquid phase). Due to the permeable capillary effect of
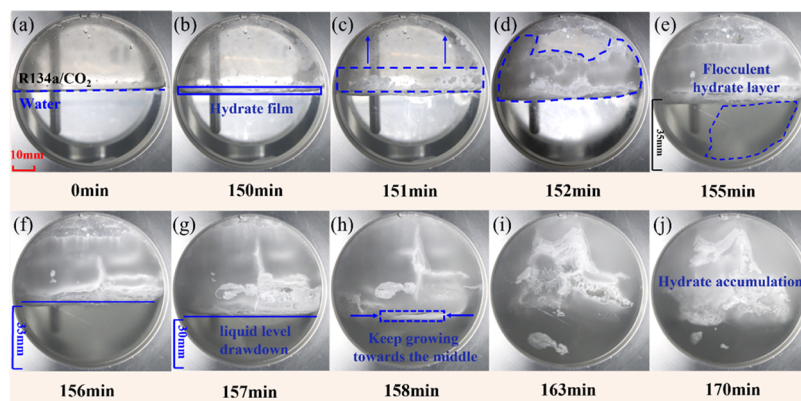
**Figure 8.** 7%R134$a$/93%CO$_2$ hydrate growth process with the addition of 300 ppm of SDS.
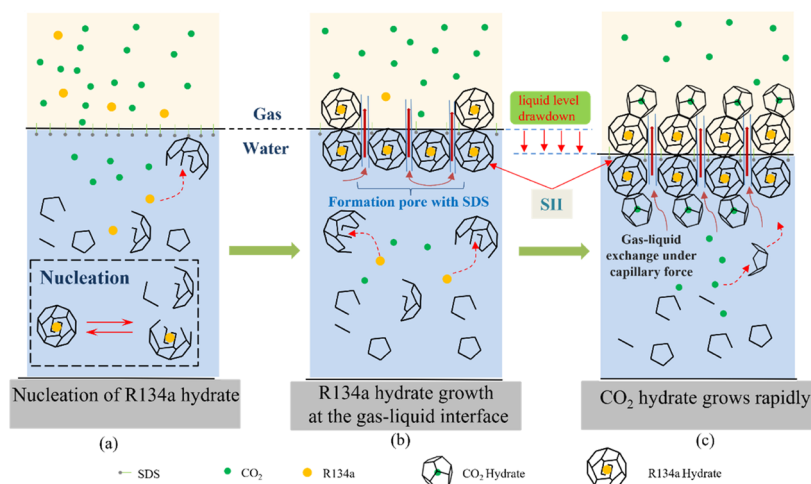


**Figure 9.** Schematic diagram of the R134a/CO$_2$ hydrate growth model with the addition of 300 ppm of SDS solution.

R134a hydrate under the action of SDS, the capillary effect draws the solution into the upper accumulation layer of hydrate, leading to the continuous renewal of the water−liquid−gas interface, thus promoting the rapid growth of hydrates. At the same time, the R134a mixed hydrate provides a nucleation site for the CO$_2$ hydrate, enhances the growth of the CO$_2$ hydrate, and promotes the growth rate of the hydrate and water conversion.

In the formation model of R134a/CO$_2$ hydrate under SDS in Figure 9, as the temperature decreases, SDS is an amphiphilic organic salt with both hydrophilic and hydrophobic properties on the gas−liquid interface, and its hydrocarbon tail is oriented toward the gas phase. This prevents gas from supplying to the front of the hydrate and inhibits the growth of the hydrate film at the gas−liquid interface. The neat arrangement of SDS organic salt at the gas−liquid interface (Figure 9a) shows that the R134a hydrate starts nucleation first due to relatively mild phase equilibrium conditions. The nucleation rate at the reactor wall in contact with the gas−liquid interface is faster than that at the general gas−liquid−solid contact line. As SDS adsorbed on the reaction wall, a large amount of R134a hydrate is formed in the upper part of the gas−liquid interface, and the porous capillary effect caused hydrate crystals. Under the action of SDS, R134a forms a porous hydrate channel at the gas−liquid interface, and the gas hydrate delivers SDS solution to the porous hydrate through a capillary mechanism and grows along

the wall (Figure 9b). The growth rate of hydrate increases with the increase of gas−liquid (or liquid−solid) interface area. CO$_2$ hydrate begins to grow and aggregates around R134a hydrate crystals. R134a hydrate provides nucleation sites for the formation of CO$_2$ hydrate, which enhances the growth of the CO$_2$ hydrate, accompanied by a decrease in solution level (Figure 9c). This also explains the two temperature peaks on the P−T curve. As the reaction progresses, the gas pressure decreases, the hydrate forms completely, and the reaction ends. This paper summarizes the mechanism model of the rapid formation of CO$_2$ hydrate promoted by the addition of trace gas promoter R134a, which provides a new method and guidance for CO$_2$ storage.

## 4. RESULTS AND DISCUSSION

This study aimed to investigate the impact of various R134a concentrations on the growth of CO$_2$ hydrate growth. Additionally, experiments were conducted to explore the enhancement of hydrate growth in the R134a/CO$_2$ mixture through stirring and the addition of SDS, with visualization used for observation. The experimental findings are outlined below:

(1) Trace R134a promoted the rapid formation of CO$_2$ hydrate. With the increase of R134a concentration, the formation of hydrate first increased and then decreased, the gas consumption of 7%R134$a$/93%CO$_2$ hydrate

formation is the largest, and the average gas consumption is 0.302 mmol/mol water.

(2) Both stirring and SDS promoted the nucleation of $CO_2$ hydrate, shortened the induction time, and increased the growth rate. Among them, the addition of stirring and SDS in 7%R134a/93%$CO_2$ increased hydrate formation from 0.31 to 0.34 mol and 0.54 mol, respectively, representing a 9 and 44% increase in hydrate gas consumption.

(3) A special phenomenon is found that when stirring or SDS is added to the mixed gas reaction system, two temperature peaks appear on the hydrate formation temperature curve, corresponding to two different stages of hydrate formation. In the first stage, R134a hydrate is preferentially formed. In the second stage, a large amount of $CO_2$ hydrate is formed.

(4) The growth model of rapid $CO_2$ hydrate formation promoted by trace R134a combined with SDS was summarized. Under the action of SDS, R134a hydrate is first formed, which is mainly deposited on the gas−liquid interface and the reactor wall in the form of porous hydrate. The capillary drive mechanism provides continuous gas−liquid exchange and promotes the growth of $CO_2$ hydrate.

## ■ AUTHOR INFORMATION

**Corresponding Authors**

**Jinhai Zhang** − *School of Energy and Power Engineering, Zhengzhou University of Light Industry, Zhengzhou 450002, China*; Email: 568028381@qq.com

**Chuanxiao Cheng** − *School of Energy and Power Engineering, Zhengzhou University of Light Industry, Zhengzhou 450002, China*; ⊙ orcid.org/0000-0001-5057-6364; Email: ccxring@gmail.com

**Authors**

**Tianyi Song** − *School of Energy and Power Engineering, Zhengzhou University of Light Industry, Zhengzhou 450002, China; Longhua Technology Group (Luoyang) Co., Ltd., LuoYang 471026, China*

**Wei Li** − *Longhua Technology Group (Luoyang) Co., Ltd., LuoYang 471026, China*

**Jie Ma** − *Longhua Technology Group (Luoyang) Co., Ltd., LuoYang 471026, China*

**Shen Hu** − *Longhua Technology Group (Luoyang) Co., Ltd., LuoYang 471026, China*

**Jianxiu Liu** − *School of Energy and Power Engineering, Zhengzhou University of Light Industry, Zhengzhou 450002, China*

**Xiaonan Li** − *School of Energy and Power Engineering, Zhengzhou University of Light Industry, Zhengzhou 450002, China*

**Wenfeng Hu** − *School of Energy and Power Engineering, Zhengzhou University of Light Industry, Zhengzhou 450002, China*

**Chunming Lan** − *Longhua Technology Group (Luoyang) Co., Ltd., LuoYang 471026, China*

**Guohua Tian** − *Longhua Technology Group (Luoyang) Co., Ltd., LuoYang 471026, China*

**Tingxiang Jin** − *School of Energy and Power Engineering, Zhengzhou University of Light Industry, Zhengzhou 450002, China*; ⊙ orcid.org/0000-0001-8883-8294

**Yuexin Han** − *School of Energy and Power Engineering, Zhengzhou University of Light Industry, Zhengzhou 450002, China*

**Jiancheng Wang** − *School of Energy and Power Engineering, Zhengzhou University of Light Industry, Zhengzhou 450002, China*

**Junjie Gong** − *School of Energy and Power Engineering, Zhengzhou University of Light Industry, Zhengzhou 450002, China*

Complete contact information is available at:
https://pubs.acs.org/10.1021/acsomega.3c04578

## Notes

The authors declare no competing financial interest.

## ■ REFERENCES

(1) Ma, Z. W.; Zhang, P.; Bao, H. S.; Deng, S. Review of fundamental properties of CO2 hydrates and CO2 capture and separation using hydration method. *Renewable Sustainable Energy Rev.* **2016**, *53*, 1273−1302.

(2) Li, S.; Deng, S.; Zhao, L.; Zhao, R.; Lin, M.; Du, Y.; Lian, Y. Mathematical modeling and numerical investigation of carbon capture by adsorption: Literature review and case study. *Appl. Energy* **2018**, *221*, 437−449.

(3) Zhang, C.; Huang, M.; Zhong, S.; Qi, J.; Sui, Y.; Meng, Q.; Wei, F.; Zhu, L.; Ren, Y.; Wei, W. Controllable construction of boron and nitrogen co-doping honeycomb porous carbon as promising materials for CO2 capture and supercapacitors. *J. Energy Storage* **2022**, *55*, No. 105687, DOI: 10.1016/j.est.2022.105687. Le Moullec, Y.; Neveux, T.; Al Azki, A.; Chikukwa, A.; Hoff, K. A. Process modifications for solvent-based post-combustion CO2 capture. *Int. J. Greenhouse Gas Control* **2014**, *31*, 96−112.

(4) Lin, H.; He, Z.; Sun, Z.; Vu, J.; Ng, A.; Mohammed, M.; Kniep, J.; Merkel, T. C.; Wu, T.; Lambrecht, R. C. CO2-selective membranes for hydrogen production and CO2 capture − Part I: Membrane development. *J. Membr. Sci.* **2014**, *457*, 149−161.

(5) Song, C.; Liu, Q.; Deng, S.; Li, H.; Kitamura, Y. Cryogenic-based CO2 capture technologies: State-of-the-art developments and current challenges. *Renewable Sustainable Energy Rev.* **2019**, *101*, 265−278.

(6) Sayani, J. K. S.; English, N. J.; Khan, M. S.; Lal, B.; Kamireddi, V. R. Estimation of Thermodynamic Stability of Methane and Carbon Dioxide Hydrates in the Presence of Hydrogen Sulfide. *ACS Omega* **2023**, *8* (7), 6218−6224.

(7) Zhang, F.; Wang, X.; Wang, B.; Lou, X.; Lipiński, W. Effects of silica gel nanopores and surfactants on CO2 hydrate formation kinetics—An experimental and modeling study. *Chem. Eng. Sci.* **2022**, *262*, No. 118002, DOI: 10.1016/j.ces.2022.118002.

(8) Benmesbah, F. D.; Clain, P.; Fandino, O.; Osswald, V.; Fournaison, L.; Dicharry, C.; Ruffine, L.; Delahaye, A. Calorimetric study of carbon dioxide (CO2) hydrate formation and dissociation processes in porous media. *Chem. Eng. Sci.* **2022**, *264*, No. 118108, DOI: 10.1016/j.ces.2022.118108. Shaw, R.; Ibrahim, N. I.; Al Azki, A. The development of carbon capture and storage (CCS) in India: A critical review. *Carbon Capture Sci. Technol.* **2022**, *2*, No. 100036, DOI: 10.1016/j.ccst.2022.100036.

(9) Wang, X.; Zhang, F.; Lipiński, W. Research progress and challenges in hydrate-based carbon dioxide capture applications. *Appl. Energy* **2020**, *269*, No. 114928, DOI: 10.1016/j.apenergy.2020.114928. Liu, X.; Ren, J.; Chen, D.; Yin, Z. Comparison of SDS and L-Methionine in promoting $CO_2$ hydrate kinetics: Implication for hydrate-based $CO_2$ storage. *Chem. Eng. J.* **2022**, *438*, No. 135504, DOI: 10.1016/j.cej.2022.135504.

(10) Nandhini, R.; Sivaprakash, B.; Rajamohan, N.; Vo, D.-V. N. Carbon-free hydrogen and bioenergy production through integrated carbon capture and storage technology for achieving sustainable and circular economy— A review. *Fuel* **2023**, *342*, No. 126984, DOI: 10.1016/j.fuel.2022.126984. Skiba, S.; Chashchin, D.; Semenov, A.; Yarakhmedov, M.; Vinokurov, V.; Sagidullin, A.; Manakov, A.; Stoporev, A. Hydrate-based separation of the $CO_2$ + $H_2$ mixtures. Phase equilibria with isopropanol aqueous solutions and hydrogen solubility in $CO_2$ hydrate. *Int. J. Hydrogen Energy* **2021**, *46* (65), 32904−32913.

(11) Zheng, J.; Loganathan, N. K.; Zhao, J.; Linga, P. Clathrate hydrate formation of $CO_2$/$CH_4$ mixture at room temperature: Application to direct transport of $CO_2$-containing natural gas. *Appl. Energy* **2019**, *249*, 190−203. Xu, G.; Xu, C.-G.; Wang, M.; Cai, J.; Chen, Z.-Y.; Li, X.-S. Influence of nickel foam on kinetics and separation efficiency of hydrate-based Carbon dioxide separation. *Energy* **2021**, *231*, No. 120826, DOI: 10.1016/j.energy.2021.120826. Li, T.; Liu, N.; Huang, J. Effects of carbon nanotube on methane hydrate formation by molecular dynamics simulation. *J. Mol. Liq.* **2022**, *368*, No. 120621, DOI: 10.1016/j.molliq.2022.120621. Xu, C.-G.; Zhang, W.; Yan, K.-F.; Cai, J.; Chen, Z.-Y.; Li, X.-S. Research on micro mechanism and influence of hydrate-based methane-carbon dioxide replacement for realizing simultaneous clean energy exploitation and carbon emission reduction. *Chem. Eng. Sci.* **2022**, *248*, No. 117266, DOI: 10.1016/j.ces.2021.117266.

(12) Lv, Y.; Xia, X.; Wang, F.; Wu, X.; Cheng, C.; Zhang, L.; Yang, L.; Zhao, J.; Song, Y. Clathrate hydrate for phase change cold storage: Simulation advances and potential applications. *J. Energy Storage* **2022**, *55*, No. 105835, DOI: 10.1016/j.est.2022.105835. Yamamoto, K.; Iwai, T.; Hiraga, K.; Miyamoto, T.; Hotta, A.; Ohmura, R. Synthesis and thermophysical properties of Tetrabutylammonium picolinate hydrate as an energy storage phase change material for cold chain. *J. Energy Storage* **2022**, *55*, No. 105812, DOI: 10.1016/j.est.2022.105812. Wang, X.; Zhang, F.; Lipiński, W. Carbon dioxide hydrates for cold thermal energy storage: A review. *Sol. Energy* **2020**, *211*, 11−30.

(13) Cheng, C.; Wang, F.; Qi, T.; Xu, P.; Zhang, Q.; Zhang, Z.; He, C.; Zhang, J.; Zheng, J.; Zhao, J.; et al. Depressurization-induced changes in memory effect of hydrate reformation correlated with sediment morphology. *Energy* **2021**, *217*, No. 119374, DOI: 10.1016/j.energy.2020.119374.

(14) Yang, M.; Zheng, J.; Liu, W.; Liu, Y.; Song, Y. Effects of $C_3H_8$ on hydrate formation and dissociation for integrated $CO_2$ capture and desalination technology. *Energy* **2015**, *93*, 1971−1979.

(15) Zheng, J.-n.; Yang, M. Experimental investigation on novel desalination system via gas hydrate. *Desalination* **2020**, *478*, No. 114284, DOI: 10.1016/j.desal.2019.114284. Babu, P.; Nambiar, A.; Chong, Z. R.; Daraboina, N.; Albeirutty, M.; Bamaga, O. A.; Linga, P. Hydrate-based desalination (HyDesal) process employing a novel prototype design. *Chem. Eng. Sci.* **2020**, *218*, No. 115563, DOI: 10.1016/j.ces.2020.115563.

(16) Zeng, X.-Y.; Feng, J.-C.; Ke, W.; Wang, J.; Zhang, S.; Xie, Y. Film formation kinetics of Methane-propane hydrate on gas bubble in MEG and luvicap EG solutions. *Appl. Energy* **2023**, *330*, No. 120301, DOI: 10.1016/j.apenergy.2022.120301.

(17) Pefoute, E.; Martin-Gondre, L.; Ollivier, J.; Soetens, J.-C.; Russina, M.; Desmedt, A. Modeling the THF clathrate hydrate dynamics by combining molecular dynamics and quasi-elastic neutron scattering. *Chem. Phys.* **2017**, *496*, 24−34.

(18) Cheng, C.; Wang, F.; Tian, Y.; Wu, X.; Zheng, J.; Zhang, J.; Li, L.; Yang, P.; Zhao, J. Review and prospects of hydrate cold storage technology. *Renewable Sustainable Energy Rev.* **2020**, *117*, No. 109492, DOI: 10.1016/j.rser.2019.109492.

(19) Cai, J.; Zhang, Y.; Xu, C.-G.; Xia, Z.-M.; Chen, Z.-Y.; Li, X.-S. Raman spectroscopic studies on carbon dioxide separation from fuel gas via clathrate hydrate in the presence of tetrahydrofuran. *Appl. Energy* **2018**, *214*, 92−102. Phan, A.; Schlösser, H.; Striolo, A. Molecular mechanisms by which tetrahydrofuran affects $CO_2$ hydrate Growth: Implications for carbon storage. *Chem. Eng. J.* **2021**, *418*, No. 129423, DOI: 10.1016/j.cej.2021.129423.

(20) Lee, H. J.; Lee, J. D.; Linga, P.; Englezos, P.; Kim, Y. S.; Lee, M. S.; Kim, Y. D. Gas hydrate formation process for pre-combustion capture of carbon dioxide. *Energy* **2010**, *35* (6), 2729−2733.

(21) Li, Z.; Zhong, D.-L.; Zheng, W.-Y.; Yan, J.; Lu, Y.-Y.; Yi, D.-T. Morphology and kinetic investigation of TBAB/TBPB semiclathrate hydrates formed with a $CO_2$ + $CH_4$ gas mixture. *J. Cryst. Growth* **2019**, *511*, 79−88.

(22) Babu, P.; Chin, W. I.; Kumar, R.; Linga, P. The Impact of Pressure and Temperature on Tetra-n-butyl Ammonium Bromide Semi-clathrate Process for Carbon Dioxide Capture. *Energy Procedia* **2014**, *61*, 1780−1783.

(23) Wang, F.; Xia, X.; Lv, Y.; Cheng, C.; Yang, L.; Zhang, L.; Zhao, J.; Song, Y. Experimental study on the thermodynamic performance of a novel tetrabutylammonium bromide hydrate cold storage system. *J. Energy Storage* **2022**, *48*, No. 103980, DOI: 10.1016/j.est.2022.103980.

(24) Park, K. H.; Kim, D. H.; Cha, M. Structure identification of binary (cyclic alcohol guests + methane) clathrate hydrates using Rietveld analysis with the direct space method. *Chem. Phys. Lett.* **2022**, *806*, No. 140054, DOI: 10.1016/j.cplett.2022.140054.

(25) Wang, M.; Sun, Z.-G.; Li, C.-H.; Zhang, A.-J.; Li, J.; Li, C.-M.; Huang, H.-F. Equilibrium Hydrate Dissociation Conditions of $CO_2$ + HCFC141b or Cyclopentane. *J. Chem. Eng. Data* **2016**, *61* (9), 3250− 3253.

(26) Lee, H.; Park, C.; Lee, E.; Lee, J. D.; Kim, Y. Effect of HFC- 134a as a Promoter of $CO_2$ Hydrate: Phase Equilibrium, Dissociation Enthalpy and Kinetics. *J. Chem. Eng. Data* **2017**, *62* (12), 4395−4400.

(27) Mok, J.; Choi, W.; Seo, Y. Evaluation of kinetic salt-enrichment behavior and separation performance of HFC-152a hydrate-based desalination using an experimental measurement and a thermodynamic correlation. *Water Res.* **2021**, *193*, No. 116882.

(28) Cheng, C.; Wang, F.; Zhang, J.; Qi, T.; Jin, T.; Zhao, J.; Zheng, J.; Li, L.; Li, L.; Yang, P.; Lv, S. Cyclic Formation Stability of 1,1,1,2- Tetrafluoroethane Hydrate in Different SDS Solution Systems and Dissociation Characteristics Using Thermal Stimulation Combined with Depressurization. *ACS Omega* **2019**, *4* (7), 11397−11407.

(29) Nesterov, A. N.; Reshetnikov, A. M. New combination of thermodynamic and kinetic promoters to enhance carbon dioxide hydrate formation under static conditions. *Chem. Eng. J.* **2019**, *378*, No. 122165.

(30) Cheng, C.; Lai, Z.; Jin, T.; Jing, Z.; Geng, W.; Qi, T.; Zhu, S.; Zhang, J.; Liu, J.; Wang, F.; et al. Rapid nucleation and growth of tetrafluoroethane hydrate in the cyclic process of boiling— condensation. *Energy* **2022**, *256*, No. 124647.

(31) Liu, X.; Li, Y.; Chen, G.-J.; Chen, D.-Y.; Sun, B.; Yin, Z. Coupling Amino Acid with THF for the Synergistic Promotion of $CO_2$ Hydrate Micro Kinetics: Implication for Hydrate-Based $CO_2$ Sequestration. *ACS Sustainable Chem. Eng.* **2023**, *11* (15), 6057− 6069.

(32) Tang, J.; Zeng, D.; Wang, C.; Chen, Y.; He, L.; Cai, N. Study on the influence of SDS and THF on hydrate-based gas separation performance. *Chem. Eng. Res. Des.* **2013**, *91* (9), 1777−1782.

(33) Zhong, D.-L.; Li, Z.; Lu, Y.-Y.; Wang, J.-L.; Yan, J. Evaluation of $CO_2$ removal from a $CO_2$+ $CH_4$ gas mixture using gas hydrate formation in liquid water and THF solutions. *Appl. Energy* **2015**, *158*, 133−141.

(34) Smith, J. M. *Introduction to Chemical Engineering Thermodynamics*, 8th ed.; Van Ness, H. C.; Abbott, M. M.; Swihart, M. T., Eds.; McGraw-Hill, 1949.

(35) Mondal, M. K.; Balsora, H. K.; Varshney, P. Progress and trends in CO2 capture/separation technologies: A review. *Energy* **2012**, *46* (1), 431−441. Lee, Y.; Moon, S.; Hong, S.; Lee, S.; Park, Y. Observation of distinct structural transformation between sI and sH gas hydrates and their kinetic properties during CO2 capture from N2 + CO2. *Chem. Eng. J.* **2020**, *389*, No. 123749, DOI: 10.1016/j.cej.2019.123749. Li, B.; Li, X.-S.; Li, G. Kinetic studies of methane hydrate formation in porous media based on experiments in a pilot-scale hydrate simulator and a new model. *Chem. Eng. Sci.* **2014**, *105*, 220−230. Babu, P.; Ho, C. Y.; Kumar, R.; Linga, P. Enhanced kinetics for the clathrate process in a fixed bed reactor in the presence of liquid promoters for pre-combustion carbon dioxide capture. *Energy* **2014**, *70*, 664−673.